Optical properties of polytype semiconductor superlattices: Bulk and surface plasmons, Raman and electron-energy-loss spectra, and finite-size effects

Pawel Hawrylak, Gunnar Eliasson, and John J. Quinn
Department of Physics, Brown University, Providence, Rhode Island 02912
(Received 16 April 1986)

We consider a finite superlattice consisting of unit cells with quantum wells filled with different types of carriers. The density-density correlation function is calculated with use of the random-phase approximation. The theory of resonant Raman scattering and inelastic electron scattering is formulated. The general theory is applied to a type-II superlattice. Raman and electron-energy-loss spectra due to bulk and surface plasmons are predicted for various system sizes.

I. INTRODUCTION

With the advancement of the molecular beam epitaxy, a variety of semiconductor superlattices can now be grown.[1] The best known examples are the type-I GaAs-$Ga_{1-x}Al_xAs$ and the type-II GaSb-InAs superlattice. Quasi-two-dimensional layers of free carriers can be generated either by modulation doping, charge transfer, or optical pumping. Collective charge-density excitations in type-I superlattices recently received considerable attention.[2–10] The density-density correlation function for a bulk, semi-infinite, and finite superlattice have been calculated. The theory of resonant Raman scattering[4,5] and electron energy loss[6] (EEL) has been formulated. Bulk plasmons have been observed experimentally[7–9] in light scattering experiments while surface plasmons still await detection.

The goal of this paper is to extend these calculations to polytype superlattices, where a rich spectrum of collective charge excitations is expected. The article is organized as follows: In Sec. II the model system is described, and in Sec. III the density-density correlation function for this system is calculated using linear density response theory. Calculations are exact and carried out analytically as long as possible. They include intersubband scattering which has been neglected previously. In Secs. IV and V the theory of Raman scattering and inelastic electron scattering (EEL) is given. The theory is illustrated in Sec. VI on the simplest example of a polytype superlattice, i.e., a type-II superlattice. Plasma modes are predicted as a function of the size of the system, and in-plane wave vector q. Special attention is paid to surface plasmons. Both Raman intensities and EEL spectra are calculated, and their evolution with the size of the system is shown. This paragraph also contains the summary of our results.

II. THE MODEL

The system consists of N unit cells, each containing M quantum wells filled with different kinds of carriers. The quantum wells are embedded in a medium with dielectric constant ϵ, occupying the space $z > -\delta$. The other half-space is filled by an insulator with a constant ϵ_0. The wells are centered at $z = la + d_m$, and contain N_B subband each, where $l = 0,1,\ldots,N-1$ is the unit-cell index, $m = 1,2,\ldots,M$ is the carrier-type index. The single-particle states are assumed to be of the form

$$|\,\mathbf{q}lmn\,\rangle = e^{i\mathbf{q}\cdot\mathbf{r}}\xi_{nm}(z - la - d_m)\ ,$$

where $n = 0,1,\ldots,N_B-1$ is the subband index, and $\mathbf{q}$ is the momentum in the plane perpendicular to the z axis. In this paper we assume that only the lowest subband is filled at $T = 0$, and carriers are localized in the wells. The assumption of the uniform background dielectric constant is a reasonable one if the dielectric constants of the constitutive layers are quite similar.

III. DENSITY-DENSITY CORRELATION FUNCTION

The density-density correlation function $\Pi(\mathbf{q},\omega,z,z')$ for a semi-infinite type-I superlattice has been calculated by us,[4,6] and by Jain and Allen for a layered electron gas.[5] It is the central quantity for calculations of Raman intensities and electron-energy-loss spectra. Our approach here is a natural extension of previous calculations to polytype superlattices. For type-I superlattices it includes intersubband scattering.

Following Ref. 4 we expand the density-density correlation function in the single-particle states. If we assume that only the lowest subband is occupied, then

$$\Pi(\mathbf{q},\omega,z,z') = \sum_{\substack{m,m'\\ l,l'\\ n,n'}} \Pi^{nn'}_{mm'}(l,l')\Psi^{m}_{n}(z - la)\Psi^{m'}_{n'}(z' - l'a)\ , \tag{3.1}$$

where

$$\Psi^{m}_{n}(z) = \xi_{mn}(z - d_m)\xi_{m0}(z - d_m)\ . \tag{3.2}$$

We will now write $\Pi^{nn'}_{mm'}(l,l')$ as a matrix $\Pi_{pp'}(l,l') = \underline{\Pi}(l,l')$, where $p = 1 + n + N_B(m-1)$. In the random-phase approximation (RPA), $\underline{\Pi}$ satisfies the integral equation

$$\underline{\Pi}(l,l') = \underline{\Pi}^0\delta_{ll'} + \sum_{l''} \underline{\Pi}^0\cdot\underline{G}(l,l'')\cdot\underline{\Pi}(l'',l')\ , \tag{3.3}$$

where $\underline{\Pi}^0$ is the polarizability of the noninteracting sys-

tem: $\underline{\Pi}^0=\underline{\Pi}^{0n}_m\delta_{mm'}\delta_{nn'}$, where $\underline{\Pi}^{0n}_m$ is the polarizability of noninteracting carriers in a well "m" due to zeroth to nth subband transitions. $\underline{G}(l,l')$ is the Coulomb interaction between the layers, including the effect of image charges and subband structure:

$$\underline{G}_{pp'}(l,l')=V_q\int_{-\delta}^{\infty}dz\int_{-\delta}^{\infty}dz'\,\Psi^n_m(z-la)\times(e^{-q|z-z'|}+\alpha e^{-q(z+z')})\times\Psi^{n'}_{m'}(z'-l'a)\,, \tag{3.4}$$

where $\alpha=[(\epsilon-\epsilon_0)/(\epsilon+\epsilon_0)]e^{-2\delta q}$ and $V_q=2\pi e^2/\epsilon q$. Following Refs. 4 and 5, we now Fourier transform all quantities, e.g.,

$$\underline{\Pi}(k,k')=\frac{1}{N}\sum_{l,l'=0}^{N-1}e^{-ikla}\underline{\Pi}(l,l')e^{ik'l'a}\,, \tag{3.5}$$

$$\underline{\Pi}(l,l')=\frac{1}{N}\sum_{k,k'}e^{ikla}\underline{\Pi}(k,k')e^{-ik'l'a}\,, \tag{3.6}$$

where $k=2\pi n/aN$, $n=1,2,\ldots,N$. The Fourier transform of Eq. (3.3) is then

$$\underline{\Pi}(k,k')=\underline{\Pi}^0\delta_{kk'}+\sum_{k''}\underline{\Pi}^0\cdot\underline{G}(k,k'')\cdot\underline{\Pi}(k'',k')\,. \tag{3.7}$$

We now decompose $\underline{G}$ and $\underline{\Pi}$ into a part diagonal in k,k', called the bulk part, and the rest, called the surface part:

$$\underline{G}(k,k')=\underline{G}_B(k)\delta_{kk'}+G_S(k,k')\,, \tag{3.8}$$

$$\underline{\Pi}(k,k')=\underline{\Pi}_B(k)\delta_{kk'}+\underline{\Pi}_S(k,k')\,. \tag{3.9}$$

The explicit forms of $G_B(k)$ and $G_S(k,k')$ are given in the Appendix. Substitution of (3.8) and (3.9) into (3.7) gives two coupled equations for $\underline{\Pi}_B$ and $\underline{\Pi}_S$:

$$\underline{\Pi}_B(k)=\underline{\Pi}^0+\underline{\Pi}^0\cdot\underline{G}_B(k)\cdot\underline{\Pi}_B(k)\,, \tag{3.10}$$

$$\underline{\Pi}_S(k,k')=\underline{\Pi}^0\cdot\underline{G}_B(k)\cdot\underline{\Pi}_S(k,k')+\underline{\Pi}^0\cdot\underline{G}_S(k,k')\cdot\underline{\Pi}_B(k')+\sum_{k''}\underline{\Pi}^0\cdot\underline{G}_S(k,k'')\cdot\underline{\Pi}_S(k'',k')\,. \tag{3.11}$$

Equation (3.10) can readily be solved to give

$$\underline{\Pi}_B(k)=[\underline{1}-\underline{\Pi}^0\cdot\underline{G}_B(k)]^{-1}\cdot\underline{\Pi}^0 \tag{3.12}$$

We now make the ansatz for $\underline{\Pi}_S(k,k')$:

$$\underline{\Pi}_S(k,k')=\frac{1-e^{-qaN}}{4NP(k)P(k')}\underline{\Pi}_B(k)\cdot(\underline{A}-\underline{B}_1e^{ika}-\underline{B}_2e^{-ik'a}+\underline{C}e^{i(k-k')a})\cdot\underline{\Pi}_B(k')\,, \tag{3.13}$$

where $P(k)=\cosh(qa)-\cos(ka)$. Equations (3.11), (3.12), and (3.13) give four matrix equations for the coefficients $\underline{A}$, $\underline{B}_1$, $\underline{B}_2$, and $\underline{C}$, and the details are given in the Appendix.

Poles of the density-density correlation function $\underline{\Pi}(k,k')$ define collective excitations of the superlattice. When the number of layers N is very large ($N\to\infty$), bulk plasmons are given by the poles of the bulk part while surface plasmons are given by the poles of the surface part. For finite number of layers full solution must be used. An advantage of the Fourier transform method developed here is that the amount of numerical work increases only linearly with the number of layers, and that in certain special cases [layered electron gas (LEG), type-I superlattice without intersubband scattering] it permits exact and analytical solutions.[4–6] The success of the method lies in the fact that the Coulomb interaction matrix $\underline{G}(k,k')$ can be factorized. This point is well explained in Ref. 10.

IV. RAMAN INTENSITIES

The Raman intensity is proportional[4,5] to the function $F(\omega,Q)$ in Eq. (4.1). This function contains the imaginary part of the density-density correlation function, which has been calculated in the previous section. We assume that the energy of the incoming light is close to the band gap for one kind of carriers as in a previous analysis for type-I superlattice.[4] This means that the light will couple essentially to that type of carrier. In our calculations we assume that the light only couples to one kind of carrier "m," so only $\mathrm{Im}\{\sum_{nn'}\Pi^{nn'}_{mm}(l,l')\}$ is included in the expression for $F(\omega,Q)$. If the incoming and scattered light have frequencies and wave vectors $(\omega_i,\mathbf{q}_i,k_z^i)$ and $(\omega_s,\mathbf{q}_s,-k_z^s)$, then at $T=0$:

$$F(\omega,\mathbf{Q})=\int_{-\delta}^{\infty}dz\int_{-\delta}^{\infty}dz'\,e^{-ik_z^*z}e^{ik_zz'}\times\mathrm{Im}\{-[\Pi(z,z',\mathbf{q},\omega)]_{mm}\}\,, \tag{4.1}$$

where

$$\omega=\omega_i-\omega_s$$

and

$$\mathbf{Q}=(\mathbf{q},k_z)=(\mathbf{q}_i-\mathbf{q}_s,k_z^i+k_z^s)\,.$$

We now make the approximation

$$k_z^i=k_z^s=k+\frac{i}{2\lambda}\,,$$

where

$$k=\frac{\omega_i}{c}\mathrm{Re}\sqrt{\epsilon}\,,$$

$$\frac{1}{\lambda}=\frac{2\omega_i}{c}\mathrm{Im}\sqrt{\epsilon}\,,$$

$2k$ is thus the momentum transfer to the plasmon from a photon along the superlattice axis, and λ is the photon decay length inside the material.

The function $F(\omega,Q)$ then becomes

$$F(\omega,\mathbf{Q})=-\sum_{l,l'}\sum_{n,n'}e^{-2\delta/\lambda}\int_{-\delta}^{\infty}dz\int_{-\delta}^{\infty}dz'\,e^{-2ik(z-z')}e^{-(z+z')/\lambda}\mathrm{Im}\{\Pi^{nn'}_{mm}(l,l')\}\Psi^m_n(z-la)\Psi^m_{n'}(z'-l'a)$$
$$=-\sum_{l,l'}\sum_{n,n'}\mathrm{Im}\{\Pi^{nn'}_{mm}(l,l')\}S^{nn'}_{mm}(l,l')\,, \tag{4.2}$$

where

$$S_{mm'}^{nn'}(l,l')=e^{-2\delta/\lambda}\int dz\int dz'\,e^{-2ik(z-z')}e^{-(z+z')/\lambda}\times\Psi_n^m(z-la)\Psi_{n'}^{m'}(z'-l'a) \tag{4.3}$$

is the structure factor.

V. ELECTRON ENERGY LOSS

Electron-energy-loss spectroscopy can be used to probe surface collective modes of a superlattice. The theory of the inelastic electron scattering from the surface of type-I superlattice has been given by us recently.[6] Here we extend this calculation to a polytype superlattice.

As in the case of Raman scattering, the response function for electron scattering R is proportional to the imaginary part of the density-density correlation function. In contrast to light scattering, the incoming electrons couple to all carriers.

The response function $R(\mathbf{q},\omega)$ of the system is derived using a semiclassical approach of Schaich[11] and Camley and Mills.[12] The probability $P(\mathbf{q},\omega)d\omega\,d^2q$ that the electron is inelastically scattered into the range of energy loss $\hbar(\omega+d\omega)$ and in-plane momentum loss $\hbar(\mathbf{q}+d\mathbf{q})$ is[6]

$$P(\mathbf{q},\omega)=\frac{4e^2v_z^2q}{\hbar\pi^2}\frac{\mathrm{Im}[-R(\mathbf{q},\omega)]}{[q^2v_z^2+(\omega-\mathbf{q}\cdot\mathbf{v}_{||})^2]^2}\ , \tag{5.1}$$

where $\mathbf{v}=(\mathbf{v}_{||},v_z)$ is the velocity of the incoming electrons. The response function $R(q,\omega)$ is calculated by matching the boundary conditions for the electric potential from the incoming electrons, and the potential due to induced density fluctuations in the material. A straightforward extension of the derivation in Ref. 6 to a polytype superlattice gives us

$$R(\mathbf{q},\omega)=\frac{1+\alpha}{1+\epsilon}\sum_{l,l'=0}^{N-1}\mathbf{S}\cdot\underline{\Pi}(l,l')\cdot\mathbf{S}e^{-qal}e^{-qal'}+\frac{1}{\epsilon+1}-1\ , \tag{5.2}$$

where the structure factor is

$$S_p=\int_{-\delta}^{\infty}dz\,e^{-qz}\xi_{mn}(z-d_m)\xi_{m0}(z-d_m)\ . \tag{5.3}$$

VI. RESULTS AND CONCLUSIONS

As an illustration of the formalism, we have chosen the simplest example of a polytype superlattice, i.e., type-II superlattice. The type-II superlattice consists of alternating layers of electrons and holes. We have taken the first layer to be a hole layer, and set $d_1=0$ for holes, and $d_2=0.5a$ for electrons. The surface modes of this system in the electric quantum limit have been studied by Qin, Giuliani, and Quinn.[13] An interesting possibility of an acoustical intrasubband surface plasmon has been predicted. To study this effect in greater detail, we will only consider intrasubband modes here, and neglect subband structure. This is a good approximation for these modes. The densities in the z direction are thus taken as δ functions. The background dielectric has been given the values $\epsilon=13.1$ and $\epsilon_0=1$, and the distance from the first layer to the interface is $\delta=0$. We have furthermore used the long wavelength form of $\Pi_m^0(q,\omega)$:

$$\Pi_{e,h}^0=\frac{n_{e,h}q^2}{m_{e,h}(\omega^2+i\gamma\omega)}\ ,$$

where γ is the phenomenological broadening. The ratio of the plasma frequencies for the electron layers, and the hole layers, is $r=\omega_e^2/\omega_h^2$.

First we consider the dispersion of the collective modes. The plasmons correspond to poles in the density-density correlation function $\underline{\Pi}$. For a system of N cells and M types of carriers, there are $N\times M$ intersubband modes. Figure 1 shows ω versus qa for a system with ten unit cells, where ω is in units of

$$\omega_h=\left[\frac{2\pi n_h e^2}{m_h\epsilon a}\right]^{1/2}$$

and $r=2$. The shaded areas are the two bulk modes, and S_1 and S_2 are the surface modes for a semi-infinite system. The surface modes of the finite system are indistinguishable from the semi-infinite system. The distribution of the 20 modes is nine in each bulk region, and two surface modes. The modes in the upper bulk region are

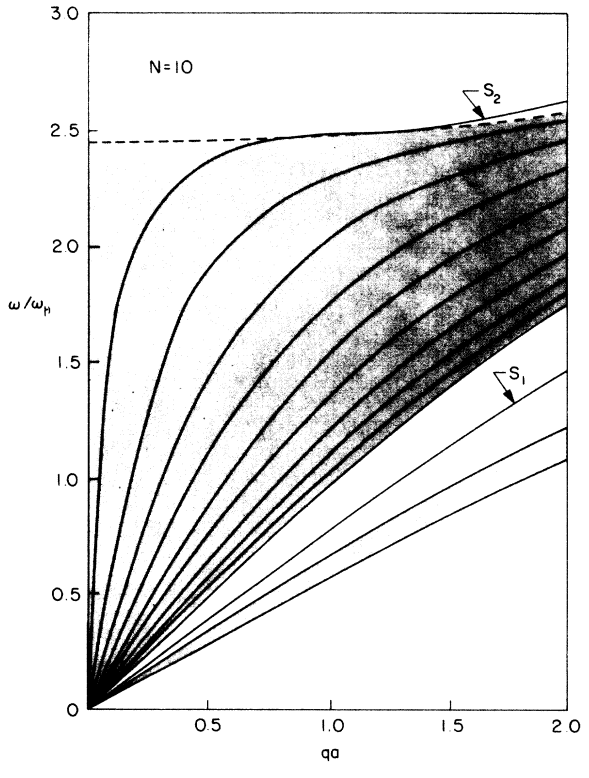

FIG. 1. Dispersion relation ω vs qa for a type-II superlattice with ten unit cells, the first layer containing holes. The shaded areas are the bulk modes for an infinite system. The solid lines in the upper bulk regions are the modes of the finite system. S_1 and S_2 are the two surface modes. The parameters are $\epsilon=13.1$, $\epsilon_0=1.0$, $\delta=0$, $r=2.0$, $d_1=0$, and $d_2=0.5a$.

drawn in the figure. In between the bulk regions is an acoustical surface mode, discovered by Qin *et al.*[13] This mode only exists for $r > 1$. Figure 2 shows how the distribution of modes changes with N, at $qa = 1$. (Note the change in energy scale.) The surface modes converge very rapidly to their large N limit. From this analysis we conclude that the system can be well approximated by a semi-infinite one for the surface mode for almost all N and wave vector q. The predictions for a high-frequency surface mode are valid for $qa > 1$.

We now turn to Raman intensities. The light is assumed to couple only to the holes, and the parameters used are $\delta = 0$, $\gamma = 0.05\omega_h$, $ka = 5.5$, and $\lambda = 6.0a$. Figure 3 shows the logarithm of the Raman intensity versus ω, the energy loss of the scattered light, for three different system sizes: $N = 4$, 10, and 40. The in-plane momentum transfer is $qa = 1.0$. The peaks in the spectrum correspond to the poles of the polarizability matrix $\underline{\Pi}$. For $N = 4$ (top curve) there are six peaks visible. The highest peak corresponds to three holelike modes with frequencies closely spaced (see Fig. 2) and lying within a bulk holelike plasmon band. The next peak corresponds to the mode with frequency between holelike and electronlike plasmon bands which evolves to an acoustical surface mode as the system size N increases. The next three modes are within an electronlike plasmon band. Their energy difference is much larger than that of holelike modes hence they are clearly visible. The last mode with highest frequency is outside the electronlike plasmon band spectrum and evolves into a high-fequency surface mode as the system size increases. This process is illustrated by Raman intensities for the system sizes $N = 10$ and $N = 40$. For $N = 40$ only four peaks are well resolved. The first and the third

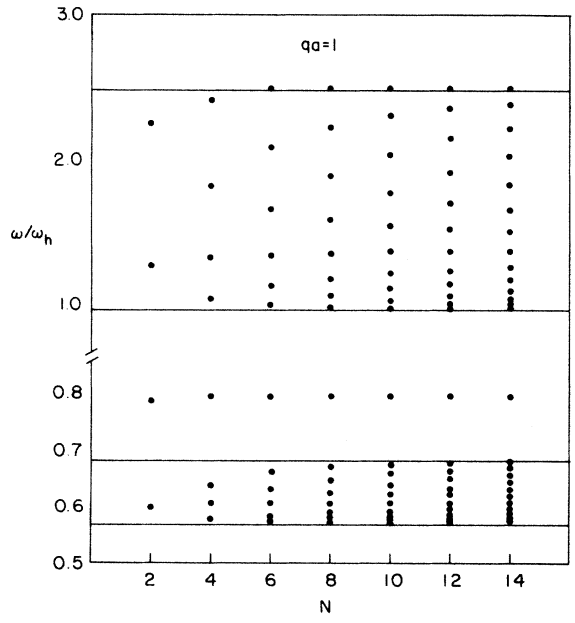

FIG. 2. Energies of modes as a function of the number of unit cells. The solid lines are the band edges of the bulk modes. The parameters used are the same as in Fig. 1.

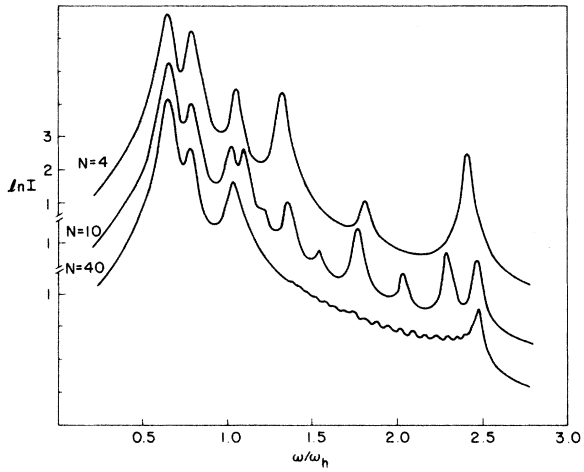

FIG. 3. Logarithm of the Raman intensity versus the energy transfer ω, for three system sizes, $N = 4$, 10, and 40. The in-plane momentum transfer $qa = 1.0$. The parameters are the same as in Fig. 1. Other parameters are $ka = 5.5$, $\lambda = 6.0a$, and $\gamma = 0.05\omega_h$.

(counting from the left) correspond to the modes of the bulk (infinite) spectrum with momentum along the superlattice axis equal to the change of the photon momentum. The second and the fourth are an acoustical and optical surface mode. The oscillating behavior in the bulk, high-frequency, electronlike spectrum is due to the discrete nature of the spectrum. The quantization of the plasmon spectra for a type-I superlattice has been recently observed experimentally by Pinczuk *et al.*[9] and discussed theoretically by Jain and Allen.[5] Note from Fig. 3 that the holelike bulk surface plasmons show higher intensities than the electronlike plasmons. This is because we have assumed that the incoming photon excites directly only plasmons on hole layers.

Finally we calculate EEL spectrum. Figure 4 shows the logarithm of the intensity versus the energy loss ω, for the

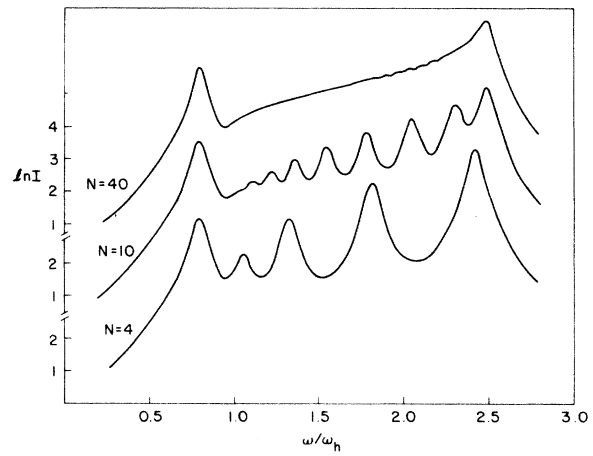

FIG. 4. Logarithm of $I = \mathrm{Im}[-R(q,\omega)]$ versus the energy loss ω for inelastic electron scattering on the same systems as in Fig. 3. The in-plane momentum loss is kept at $qa = 1.0$, and $\gamma = 0.1\omega_h$.

system sizes $N=4$, 10, and 40. For better comparison with Raman spectrum we plot the spectral function $I(q,\omega)=\mathrm{Im}[-R(q,\omega)]$ as a function of ω for a constant q, and not the scattering probability $P(q,\omega)$ which involves a kinematic, frequency-dependent factor intrinsic to the scattering process itself. The broadening is $\gamma=0.1\omega_h$. In contrast to Raman scattering which couples strongly to bulk modes, electron scattering couples strongly to surface modes. For large N ($N=40$ in Fig. 4) only peaks due to surface modes are well resolved. These peaks are accompanied by continuous shoulders due to excitation of bulk modes. Note that while acoustical surface mode had higher intensity than the high-frequency surface mode in the Raman spectrum, the situation is reversed in the EEL spectrum. We must keep in mind that the EEL spectrum excites all modes of the system on equal footing while the light scattering excited only hole-like modes directly.

In summary, we have extended previous theories of collective charge excitations to polytype semiconductor superlattices. The density-density correlation function has been calculated and plasmon modes predicted. Our formalism allows for finite-size effects and intersubband scattering. The theory of Raman scattering and inelastic electron scattering has been formulated. As an example of the formalism, intrasubband plasma modes of a type-II superlattice have been studied and their Raman and EEL spectra predicted.

ACKNOWLEDGMENTS

The authors wish to acknowledge the support of the U.S. Army Research Office (Durham, NC). One of us (G.E.) wishes to acknowledge support from IBM.

APPENDIX

The bulk surface parts of $\underline{G}(k,k')$ are, respectively,

$$\underline{G}_B(k)=[\underline{g}_-(q)(e^{-ika}-e^{-qa}) +\underline{g}_-(-q)(e^{ika}-e^{-qa})]\frac{1}{2P(k)}+\underline{V}(q)\ , \quad \text{(A1)}$$

where

$$g_{\pm pp'}(q)=e^{-q(d_m\pm d_{m'})}\int_{-\delta}^{\infty}dz\int_{-\delta}^{\infty}dz'\,\Psi_m^n(z)\times e^{-q(z\pm z')}\Psi_{m'}^{n'}(z')\ , \quad \text{(A2)}$$

$$V_{pp'}(q)=\int_{-\delta}^{\infty}dz\int_{-\delta}^{\infty}dz'\,\Psi_m^n(z)e^{-q|z-z'+d_m-d_{m'}|}\times\Psi_{m'}^{n'}(z')\ , \quad \text{(A3)}$$

and

$$\underline{G}_S(k,k')=\frac{1-e^{-qaN}}{4NP(k)P(k')}\times(\underline{a}-\underline{b}_1e^{ika}-\underline{b}_2e^{-ik'a}+\underline{c}e^{i(k-k')a})\ , \quad \text{(A4)}$$

$$\underline{a}=\underline{g}_-(q)+\underline{g}_-(-q)+\tilde{\alpha}\underline{g}_+(q)e^{2qa}\ , \quad \text{(A5)}$$

$$\underline{b}_1=\underline{g}_-(q)e^{-qa}+\underline{g}_-(-q)e^{qa}+\tilde{\alpha}\underline{g}_+(q)e^{qa}\ , \quad \text{(A6)}$$

$$\underline{b}_2=\underline{g}_-(q)e^{qa}+\underline{g}(-q)e^{-qa}+\tilde{\alpha}\underline{g}_+(q)e^{qa}\ , \quad \text{(A7)}$$

$$\underline{c}=\underline{g}_-(q)+\underline{g}_-(-q)+\tilde{\alpha}\underline{g}_+(q)\ , \quad \text{(A8)}$$

$$\tilde{\alpha}=(1-e^{-qaN})\alpha\ . \quad \text{(A9)}$$

The ansatz (3.13) in Eq. (3.11) gives, after some algebra, two coupled equations for $\underline{A}$, $\underline{B}_1$, $\underline{B}_2$, and $\underline{C}$:

$$M\begin{bmatrix}\underline{A}\\ \underline{B}_1\end{bmatrix}=\begin{bmatrix}\underline{a}\\ \underline{b}_1\end{bmatrix}\ \text{and}\ M\begin{bmatrix}\underline{B}_1\\ \underline{C}\end{bmatrix}=\begin{bmatrix}\underline{b}_1\\ \underline{c}\end{bmatrix}\ , \quad \text{(A10)}$$

where

$$M=\begin{bmatrix}\underline{1}-\underline{a}\cdot\underline{G}-\underline{b}_2\cdot\underline{H}_- & \underline{a}\cdot\underline{H}_+-\underline{b}_2\cdot\underline{G}\\ \underline{c}\cdot\underline{H}_--\underline{b}_1\cdot\underline{G} & \underline{1}-\underline{c}\cdot\underline{G}+\underline{b}_1\cdot\underline{H}_+\end{bmatrix}\ , \quad \text{(A11)}$$

$$\underline{G}=\frac{V_q(1-e^{-qaN})}{4N}\sum_k\frac{1}{P(k)^2}\underline{\Pi}_B(k)\ , \quad \text{(A12)}$$

$$\underline{H}_\pm=\frac{V_q(1-e^{-qaN})}{4N}\sum_k\frac{e^{\pm ika}}{P(k)^2}\underline{\Pi}_B(k)\ . \quad \text{(A13)}$$

The matrix M is then inverted numerically to evaluate $\underline{A}$, $\underline{B}_1$, $\underline{B}_2$, and $\underline{C}$.

[1]L. Esaki, in *Proceedings of the 17th International Conference on the Physics of Semiconductors, San Fransisco, 1984,* edited by J. D. Chadi and W. A. Harrison (Springer, New York, 1985), p. 473.
[2]A. C. Tselis and J. J. Quinn, Phys. Rev. B **29**, 3318 (1984).
[3]G. F. Giuliani and J. J. Quinn, Phys. Rev. Lett. **51**, 919 (1983).
[4]P. Hawrylak, J.-W. Wu, and J. J. Quinn, Phys. Rev. B **32**, 5162 (1985); **31**, 7855 (1985).
[5]J. K. Jain and P. B. Allen, Phys. Rev. Lett. **54**, 947 (1985); Phys. Rev. B **32**, 997 (1985); Phys. Rev. Lett. **54**, 2437 (1985).
[6]P. Hawrylak, J.-W. Wu, and J. J. Quinn, Phys. Rev. B **32**, 4272 (1985).
[7]D. Olego, A. Pinczuk, A. C. Gossard, and W. Wiegmann, Phys. Rev. B **25**, 7867 (1982).
[8]R. Sooryakumar, A. Pinczuk, A. Gossard, and W. Wiegmann, Phys. Rev. B **31**, 2578 (1985).
[9]A. Pinczuk, M. G. Lamont, and A. C. Gossard, Phys. Rev. Lett. **56**, 2092 (1986).
[10]P. Hawrylak and J. J. Quinn (unpublished).
[11]W. L. Shaich, Phys. Rev. B **24**, 686 (1981).
[12]R. E. Camley and D. L. Mills, Phys. Rev. B **29**, 1695 (1984).
[13]G. Qin, G. F. Giuliani, and J. J. Quinn, Phys. Rev. B **28**, 6144 (1983).

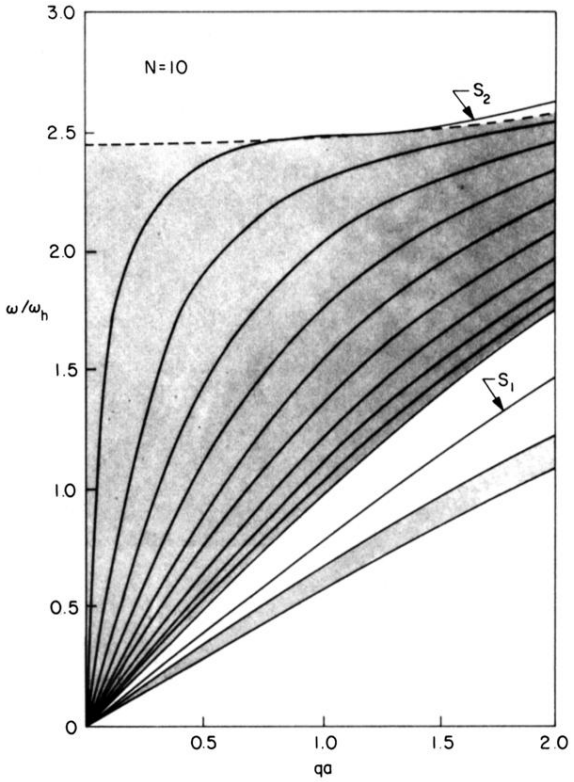

FIG. 1. Dispersion relation ω vs qa for a type-II superlattice with ten unit cells, the first layer containing holes. The shaded areas are the bulk modes for an infinite system. The solid lines in the upper bulk regions are the modes of the finite system. S_1 and S_2 are the two surface modes. The parameters are $\epsilon=13.1$, $\epsilon_0=1.0$, $\delta=0$, $r=2.0$, $d_1=0$, and $d_2=0.5a$.